Carrier dynamics in nitride-based light-emitting *p-n* junction diodes with two active regions emitting at different wavelengths

Y.-L. Li, Th. Gessmann, and E. F. Schubert[a)]
Department of Electrical, Computer, and Systems Engineering, Rensselaer Polytechnic Institute, Troy, New York 12180

J. K. Sheu
Optical Science Center, National Central University, Chung-Li, Taiwan, Republic of China

(Received 28 March 2003; accepted 21 May 2003)

The carrier transport and recombination dynamics of monolithic InGaN/GaN light-emitting *p-n* junction structures with two active regions are investigated. Room-temperature and low-temperature photoluminescence and room-temperature electroluminescence measurements show two emission bands originating from the two active regions. In electroluminescence, the intensity ratio of the two emission bands is independent of injection current. In contrast, the intensity ratio depends strongly on the excitation intensity in photoluminescence measurements. The dependency of the emission on excitation is discussed and attributed to carrier transport between the two active regions and to the different carrier injection dynamics in photoluminescence and electroluminescence. The luminous efficacy of a Gaussian dichromatic white-light source is calculated assuming a line broadening ranging from $2kT$ to $10kT$. Luminous efficacies ranging from 380 to 440 lm/W are obtained for broadened dichromatic sources. © *2003 American Institute of Physics.*
[DOI: 10.1063/1.1591051]

I. INTRODUCTION

Nitride-based light-emitting diodes (LED's) are suitable for many applications including signage, display, and lighting applications. For these applications, efficient generation of white light is very desirable. White light can be generated by two or more LED sources emitting complementary colors, or by LED's exciting wavelength converters such as phosphors,[1,2] dyes,[3] or semiconductors.[4] It has been shown that the most energy-efficient way to generate white light is the mixing of two narrow emission lines, namely, one in the blue and one in the green region of the visible spectrum.[5,6] Mixing monochromatic emission lines at 450 and 570 nm,[5] with an intensity ratio of $I(450\,\text{nm})/I(570\,\text{nm})=1.79$,[7] gives a luminous efficacy of more than 400 lm/W.[5] Such dichromatic white light sources are very well suited for signage applications due to their high efficacy and the irrelevancy of color rendering in signage applications. However, dichromatic light sources are not suited for daylight illumination applications due to their low color rendering.[8] It is well known that there is a fundamental trade-off between high luminous efficacy and color rendering. As a consequence, the highest-luminous-efficacy sources necessarily have a low color rendering index.

Efficient and monolithic solid-state white light sources can be demonstrated by using quantum well structures emitting at two or more wavelengths. It is important to understand the carrier dynamics of such quantum-well structures to improve the performance of the devices.[9,10] In this article, the optical characteristics of a monolithic *p-n* junction LED with two quantum-well active regions are investigated. The two emission wavelengths are 460 and 520 nm. At these wavelengths, active regions with high internal efficiency can be grown by metal-organic chemical vapor deposition (MOCVD). However, the wavelength pair (460 and 520 nm) is not complementary. The carrier transport and recombination dynamics of this dichromatic source are investigated. We find markedly different emission characteristics for photopumped and current-injected excitation. In photopumped experiments, the intensity ratio depends strongly on the excitation level, whereas for current injection a constant intensity ratio is found.

II. EXPERIMENTS

The InGaN/GaN LED samples were grown by MOCVD on a (0001) sapphire substrate. On top of the sapphire substrate, a 20 nm thick GaN nucleation layer was grown at low temperature followed by a thick (4 μm) *n*-type GaN buffer layer. The long-wavelength ($\lambda=520\,\text{nm}$) five-period Si-doped *n*-type InGaN/GaN multiple-quantum-well (MQW) active region grown on top of the buffer layer is followed by a thin Si-doped separation layer of *n*-type GaN (20 nm). On top of the separation layer, the short-wavelength ($\lambda=460\,\text{nm}$) five-period Si-doped *n*-type InGaN/GaN MQW active region is grown followed by a thin Mg-doped *p*-type AlGaN electron-blocking layer and a Mg-doped *p*-type GaN cladding layer (120 nm). The barrier and the well widths of the MQW's are 7.5 and 2.5 nm, respectively. The top region of the cladding layer is heavily Mg doped to facilitate Ohmic contact formation.

As-grown wafers are characterized by room-temperature and low-temperature ($T=78\,\text{K}$) photoluminescence (PL) ex-

a)Electronic mail: efschubert@rpi.edu

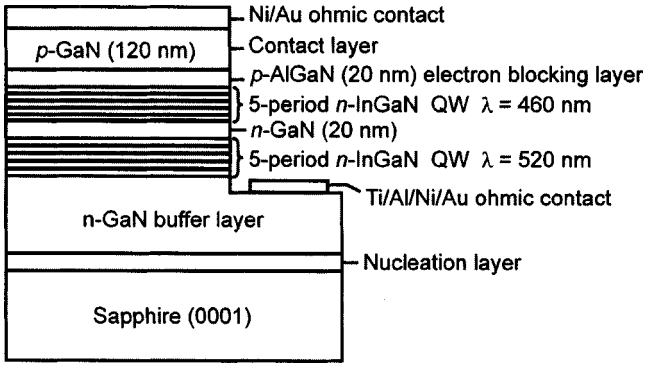

FIG. 1. The schematic structure of an InGaN/GaN LED with two active regions.

periments, pumped with a 325 nm, 50 mW He-Cd laser. The unattenuated power density of the exciting laser is $8.3\,\mathrm{kW/cm^2}$.

For processing, the samples are dipped into a diluted aqueous HCl solution (1:1) for 5 min to remove the native oxide and directly followed by Ni/Au (20 nm/20 nm) *p*-type metal contact deposition using *e*-beam evaporation. After the *p*-type contact metallization, samples are patterned by photolithography using Shipley 1813 photoresist, and etched by chemically assisted ion-beam etching with an etching rate at 25 nm/min. The *p*-type contacts are subjected to rapid thermal annealing at 530 °C for 5 min in flowing dry air. The *n*-type Ti/Al/Ni/Au (15 nm/60 nm/20 nm/20 nm) contacts are deposited on the *n*-type buffer layer right after the annealing of the *p*-type contacts. The as-deposited *n*-type contacts are of low contact resistivity (in the range of $10^5\Omega\mathrm{cm}^2$) and do not require annealing. The schematic structure of the processed samples is shown in Fig. 1.

Current-voltage (I-V) characteristics are measured with a Karl Suss probe station and a HP 4145B semiconductor parameter analyzer. The specific contact resistance of the *p*-type Ni/Au contacts, as measured by the transfer length method, was found to be in the $10^{-3}-10^{-4}\,\Omega\,\mathrm{cm}^2$ range. For electroluminescence (EL) measurements, an Ando Corp. AQ6315 optical spectrum analyzer is used.

III. RESULTS AND DISCUSSION

Room-temperature PL spectra of the two-active-region structure are shown in Fig. 2. The He-Cd laser excitation level is varied over four orders of magnitude using neutral density (ND) filters. The spectra exhibit two emission bands, one centered at about 465 and one at 525 nm. As the excitation density is varied, the two peak positions do not change. The figure also shows that the ratio of the two peak intensities changes with the power density of the laser. When the sample is pumped without a neutral density filter (i.e., with the strongest power density, $8.3\,\mathrm{kW/cm^2}$), the emission intensity of the short-wavelength (blue) peak is much stronger than that of the long-wavelength (green) peak. However, the ratio of the blue emission intensity to the green emission intensity decreases as the excitation power is decreased by neutral density filters. A ratio of one to one (i.e., equal emission intensity of the blue and green peaks) is obtained at an

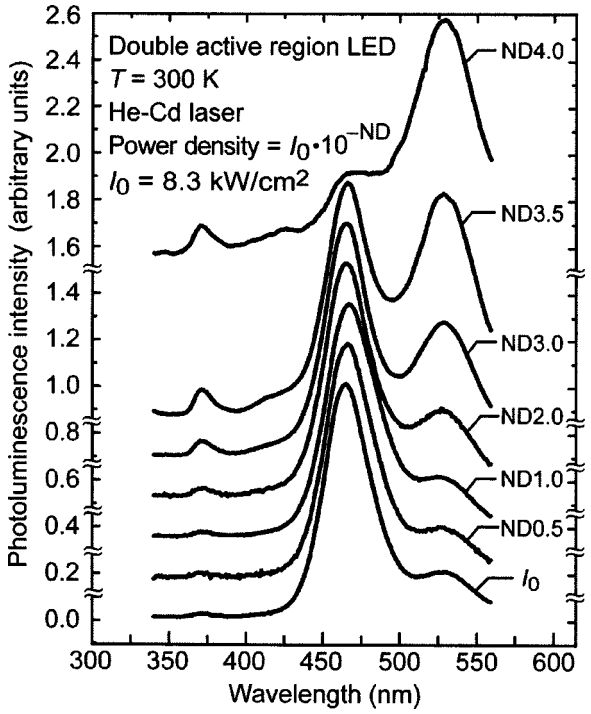

FIG. 2. The photoluminescence results with different pumping optical power density at room temperature. The ND number is the neutral density number of the applied filter.

excitation density of about $2.6\,\mathrm{W/cm^2}$ (ND=3.5). The ratio becomes even smaller than unity, i.e., higher green than blue emission intensity, at lower excitation densities.

Gaussian curves are fitted to the two peaks of the PL spectra to determine the integrated emission intensity of the two emission bands. The emission intensity versus laser power density, obtained from the PL measurements, is shown in Fig. 3. In this figure, the dashed and solid lines represent the peak and integrated values of the emission intensity, respectively, where the integrated values are deduced from the

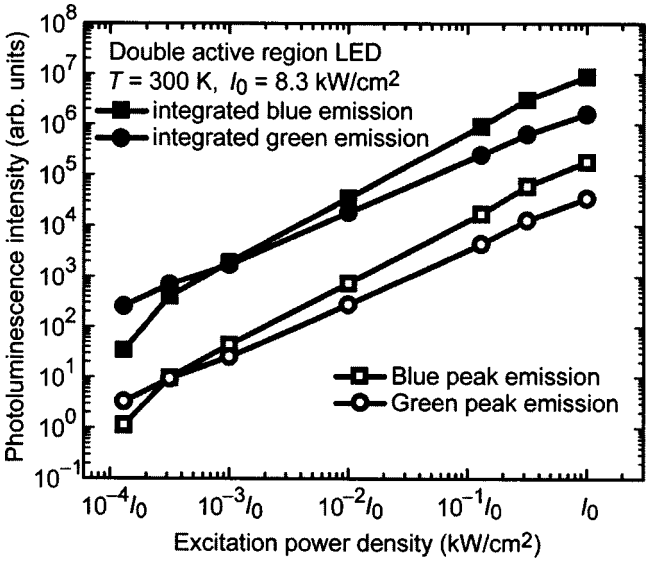

FIG. 3. The plot of the integrated and peak photoluminescence intensity vs optical power density of the pumping laser at room temperature.

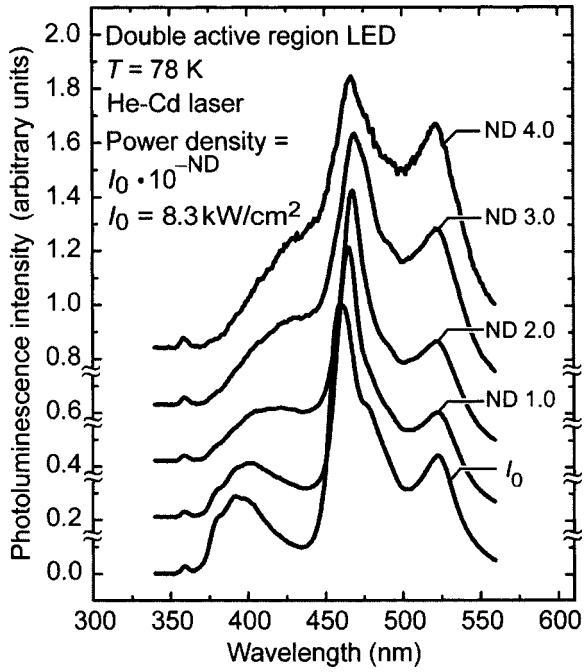

FIG. 4. The photoluminescence results with different pumping optical power densities at $T=78$ K.

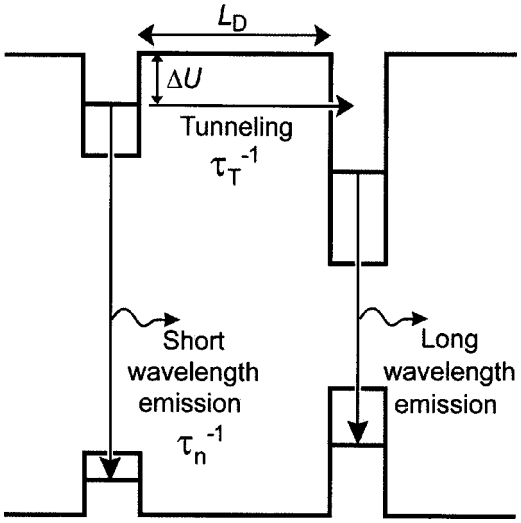

FIG. 5. The schematic tunneling mechanism for LED's with two active regions.

two Gaussian fits. The figure shows that the green emission is more intense than the blue emission at low excitation power densities.

The linewidths for the fits of the blue and green emission lines are 37 and 51 nm, corresponding to $8.1kT$ and $8.8kT$, respectively. This value is larger than $2kT$, expected for thermally broadened emission. We attribute the broader emission to alloy broadening in the InGaN QW's. A higher degree of disorder is expected for the green emission due to the higher In content, consistent with the experimental result.

PL spectra of the two-active-region structure measured at 77 K are shown in Fig. 4. Inspection of the figure and comparison with Fig. 2 reveal that the results are quite similar with respect to the peak ratios: the ratio of blue-to-green emission intensity decreases with increasing excitation power density.

The higher emission intensity of the blue peak found at high excitation densities is attributed to the fact that most of the laser power is absorbed by the top cladding layer; the ''blue QW's'' are directly adjacent to the cladding layer, in contrast to the ''green QW's.'' The absorption coefficient of GaN at 325 nm is about $1.4\times10^5\,\mathrm{cm}^{-1}$,[11] indicating that most laser power (81%) is absorbed in the 120 nm thick top cladding layer. In addition, the blue QW's have higher internal quantum efficiencies than the green QW's.[12]

The excitation-density dependent ratio of the emission line intensities can be explained by the competition of different recombination paths. Neglecting nonradiative recombination, the possible recombination path of an electron in the blue QW is either direct radiative recombination or tunneling to the green QW and subsequent radiative recombination. These two possible recombination paths are schematically shown in Fig. 5. Electrons and holes can tunnel from the blue QW to the green QW and recombine there radiatively. However, once in the green QW, carriers are unable to tunnel back to the blue QW due to the lower energy of the ground state in the green QW.

The tunneling probability T of a carrier from a blue to a green QW can be derived by the zero-order Wentzel-Kramers-Brillouin (WKB) approximation. It sensitively depends on the barrier thickness L_D and the barrier height ΔU. The tunneling probability is given by

$$T=\exp\left(-\int_0^{L_D}2\hbar^{-1}\sqrt{2m^*\Delta U}\,dx\right), \tag{1}$$

where m^* is the effective carrier mass and $\hbar$ is Planck's constant divided by 2π. The attempt rate R_a for a carrier in the blue QW to tunnel through the barrier into the green QW depends on the blue well size, L_{QW}, and the kinetic energy of the carrier. The attempt rate can be approximated as

$$R_a=\frac{1}{L_{\mathrm{QW}}}\sqrt{2E_0/m^*}, \tag{2}$$

where E_0 is the ground energy state in the blue QW. The tunneling rate R_T for one electron, which is the product of T and R_a, can be expressed as

$$R_T=\frac{\exp\left(-\int_0^{L_D}2\hbar^{-1}\sqrt{2m^*\Delta U}\,dx\right)}{L_{\mathrm{QW}}}\sqrt{2E_0/m^*}. \tag{3}$$

The tunneling rate R_T from blue to green QW's depends only on the structure of the sample but not on the carrier concentration. The lifetime for one electron in the blue QW is given by

$$\tau_T=\frac{1}{R_T}. \tag{4}$$

On the other hand, the number of radiative electron-hole recombination events per unit volume per unit time, denoted as R, is proportional to the product of hole and electron concentrations. The bimolecular rate equation is given by

$$R=Bnp, \tag{5}$$

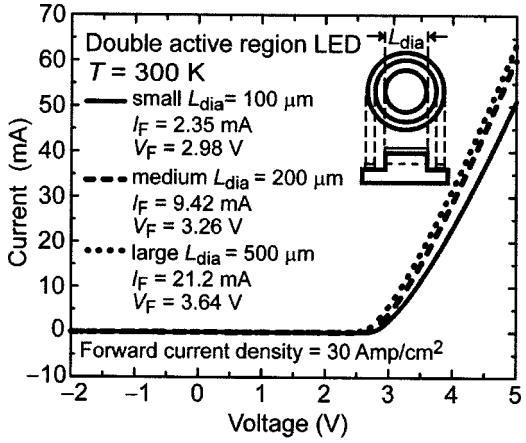

FIG. 6. Room-temperature *I-V* curves of LED's with two active regions.

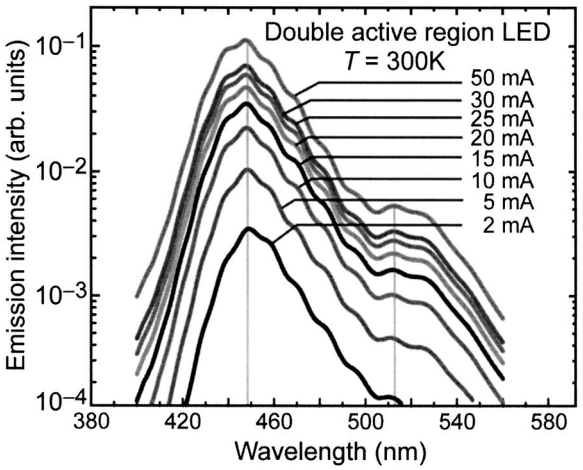

FIG. 7. Room-temperature electroluminescence results with different applied electric currents.

where n and p are the electron and hole concentrations, respectively. The proportionality constant B is the bimolecular recombination coefficient. The value of B for GaN is $2.3 \times 10^{-10}\,\mathrm{cm^3\,s^{-1}}$.[13] In the QW's, the radiative lifetime of electrons under high-level injection is given by[14]

$$\tau_n = \frac{1}{B\,\Delta p}. \tag{6}$$

Thus, by increasing the excitation power density, the number of excess carriers is increased and the lifetime of electrons is decreased through the radiative recombination process.

The ratio of the green to the blue emission intensity is given by

$$\frac{I_{\mathrm{green}}}{I_{\mathrm{blue}}} = \frac{\tau_T^{-1}}{\tau_n^{-1}}. \tag{7}$$

Note that I_{green} is proportional to τ_T^{-1} because carriers cannot tunnel back to the blue QW's after having tunneled into the green QW's. Once in the green QW's carriers must recombine in the green QW's, as mentioned previously. Because τ_n depends on the excitation intensity and τ_T is a constant, the ratio given in Eq. (7) decreases with increasing excitation intensity. The result of Eq. (7) is fully consistent with the experimental results.

Note that the barriers within each group of QW's (green and blue group) are much thinner (7.5 nm) than the barrier between the two groups (20 nm). Thus the barriers within each group of QW's can be considered as transparent for carrier transport.

Room-temperature *I-V* curves of the double-active region LED are shown in Fig. 6. We define the forward voltage (V_F) as the diode voltage at the current density of $J_F = 30\,\mathrm{A/cm^2}$. Three different circular contact sizes were used, namely, 100, 200, and 500 μm in diameter. The forward current I_F shown in the figure simply is $I_F = J_F A$, where A is the contact area. Note that excellent forward voltages below 3.0 V are obtained at small contact diameters of 100 μm, indicating high-quality Ohmic contacts. Figure 6 also shows that the forward voltage is fairly small for all contact sizes and increases with increasing contact size. The increase in forward voltage for contacts with larger diameters can be attributed to an increased voltage drop in the *n*-type buffer layer: at a given current density, the current scales with the area of the contact A, but the access resistance through the *n*-type buffer layer scales with the reciprocal circumference, that is, $A^{-1/2}$. Thus the product $V_F = RI \propto A^{-1/2} A = A^{1/2}$ increases with the area. In addition, the current crowding effect[15] leads to nonuniform current injection, particularly in large-diameter contacts, and thus to an increase in forward voltage.

The electroluminescence spectra are shown in Fig. 7. Two emission peaks are clearly observed with center wavelengths at about 455 and 520 nm. Note that the blue peak is much larger than the green peak. We attribute this to the higher quantum efficiency of blue QW's compared with green QW's. In addition, holes are injected from the blue side of the active region, whereas electrons are injected from the green side of the active region. As holes have a lower mobility and a higher effective mass, they are less likely to reach the green QW's. This can explain the higher intensity values observed for the blue emission in electroluminescence. This result is consistent with results reported by Yamada *et al.*[12]

As previously mentioned, for current injection, holes are injected into the blue QW's, and electrons are injected into the green QW's. This is very different from optical excitation, where both types of carriers are injected into the active region from both sides as well as generated inside the active region.

The EL blue and green peak intensity values versus injection current of the double-active-region LED are plotted in Fig. 8. The figure shows that the ratio of the two emission intensities does not vary with the injection current. This is a favorable property of the LED as the color of the device is constant, that is, independent of the injection current. This phenomenon is, however, different from Dalmasso *et al.*'s work,[16] where the blue and green emission ratio is dependent on the injection current. Note that there is no separation layer between the two groups of QW's in Dalmasso *et al.*'s samples. The absence of the separation layer will change the

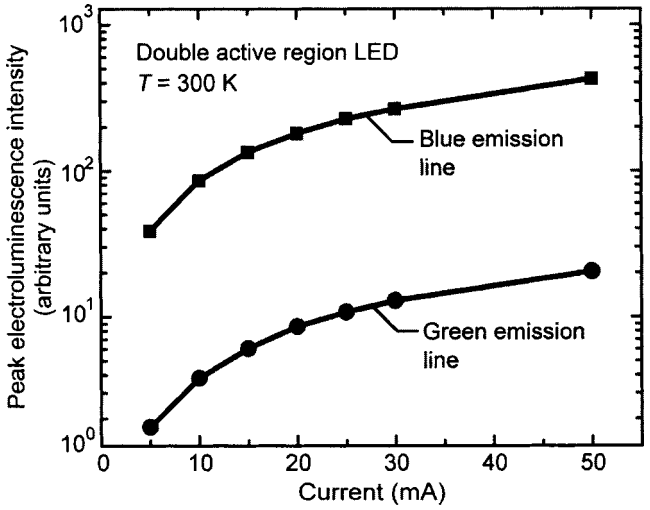

FIG. 8. The peak electroluminescence intensity plot at room temperature.

carrier dynamics by allowing a much stronger interaction of carriers in the different groups of QW's.

IV. THEORETICAL ANALYSIS OF LUMINOUS EFFICACY AND EFFICIENCY OF DOUBLE-ACTIVE-REGION LED'S

Next we analyze the luminous efficacy (luminous flux per optical unit power) and luminous efficiency (luminous flux per electrical input unit power) of a LED with two active regions emitting two lines peaked at wavelengths λ_1 and λ_2. It is assumed that the two emission lines are thermally broadened to a full width at half maximum of $\Delta E=(hc/\lambda^2)\Delta\lambda$, where ΔE ranges between $2kT$ and $10kT$. A broadening of approximately $2kT$ is expected based on thermal effects. However, broader emission lines are observed experimentally with about $8kT$ at room temperature, as discussed earlier in this article. A Gaussian line shape is assumed for the two emission bands, so that the power spectral density is given by

$$P(\lambda)=P_1\frac{1}{\sigma_1\sqrt{2\pi}}e^{-[(\lambda-\lambda_1)/\sigma_1]^2/2}+P_2\frac{1}{\sigma_2\sqrt{2\pi}}e^{-[(\lambda-\lambda_2)/\sigma_2]^2/2}, \tag{8}$$

where P_1 and P_2 are the optical powers of the two emission bands, and λ_1 and λ_2 are the peak wavelengths of the emission source. The wavelengths λ_1 and λ_2 are denoted as the primary and secondary wavelength, respectively. The standard deviation σ_1 is related to the full width at half maximum of the emission spectrum by

$$\sigma_1=\frac{\Delta\lambda_1}{2\sqrt{2\ln 2}}=\frac{\lambda_1^2\Delta E}{2hc\sqrt{2\ln 2}}. \tag{9}$$

A corresponding equation is valid for σ_2. The peak emission wavelengths λ_1 and λ_2 are chosen from Table I, which shows the wavelengths of a binary complementary source.[7] The table also gives the required power ratio of the two sources. This power ratio ensures that the emission color is white, that is, the chromaticity coordinates are of the resulting color are $x=0.3138$ and $y=0.3310$ (close to the standardized Illuminant D_{65}). Although Table I applies to strictly monochromatic light sources ($\Delta\lambda\to 0$), the data can be used, with good approximation, for light sources exhibiting moderate spectral broadening such as the LED light source considered here.

TABLE I. Complementary monochromatic wavelengths and required power ratios for a dichromatic white-light source. The wavelengths λ_1 and λ_2 are denoted as the primary and secondary wavelength, respectively

Complementary wavelengths λ_1 (nm)	λ_2 (nm)	Power ratio $P(\lambda_2)/P(\lambda_1)$	Complementary wavelengths λ_1 (nm)	λ_2 (nm)	Power ratio $P(\lambda_2)/P(\lambda_1)$
380	560.9	0.000642	460	565.9	1.53
390	560.9	0.00955	470	570.4	1.09
400	561.1	0.0785	475	575.5	0.812
410	561.3	0.356	480	584.6	0.562
420	561.7	0.891	482	591.1	0.482
430	562.2	1.42	484	602.1	0.440
440	562.9	1.79	485	611.3	0.457
450	564.0	1.79	486	629.6	0.668

Using Eqs. (8) and (9), and the data provided in Table I, the luminous efficacy can be calculated using the formula

$$\text{Luminous efficacy}=\left(683\frac{\text{lm}}{\text{W}}\int_\lambda V(\lambda)P(\lambda)d\lambda\right)\Big/\left(\int_\lambda P(\lambda)d\lambda\right), \tag{10}$$

where $V(\lambda)$ is the spectral eye sensitivity. The result of the calculation, i.e., the luminous efficacy versus primary wavelength, is shown in Fig. 9 using the Commission International de L'Eclairage (CIE) 1978 data for $V(\lambda)$, frequently referred to as the modified $V(\lambda)$ or $V_M(\lambda)$. The figure reveals that the highest luminous efficacy occurs at a primary wavelength of approximately $\lambda_1=450$ nm with a value of 439 lm/W for $\Delta E=2kT$ and 381 lm/W for $\Delta E=10kT$.

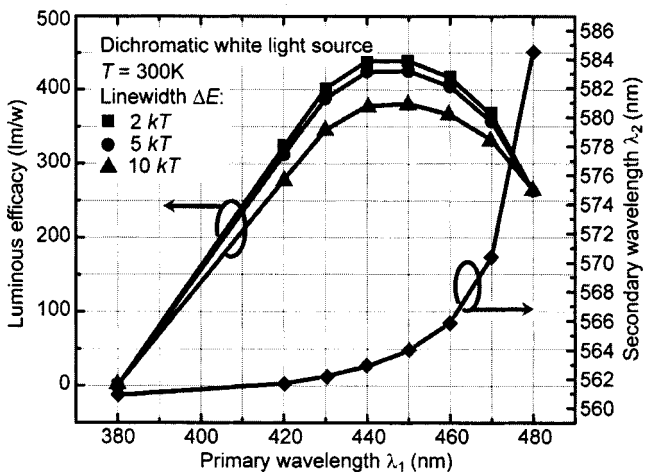

FIG. 9. Luminous efficacy calculation results on dichromatic white-light sources.

The luminous efficiency is always lower than the efficacy due to the imperfect electrical-to-optical power conversion efficiency of a LED: Denoting the power efficiency of the LED as η_{power}, the luminous efficiency is given by

$$\text{Luminous efficiency} = \eta_{\text{power}}\left(683\frac{\text{lm}}{\text{W}}\int_{\lambda} V(\lambda)P(\lambda)d\lambda\right) \Big/ \left(\int_{\lambda} p(\lambda)d\lambda\right). \tag{11}$$

To date, the best light-emitting devices have a power efficiency of about 50%. Assuming that this value of the power efficiency can be attained, the luminous efficiency of the source with $\Delta E = 2kT$ would be about 219 lm/W at the primary wavelength of $\lambda_1 = 450$ nm.

The calculation above illustrates the great potential of dichromatic light sources in terms of a very high luminous efficiency. It is important to note that such dichromatic white light sources are very well suited for large-screen display, signage, and indicator light applications, but have limited usefulness for display backlighting and general illumination applications, due to the low color rendering capabilities.

V. CONCLUSIONS

In summary, experimental results for monolithic InGaN/GaN *p-n* junction structures with two active regions have been presented. The carrier transport and recombination dynamics were investigated. Low-temperature and room-temperature photoluminescence measurements show two luminescence lines, one in the blue and one in the green part of the spectrum. The ratio of blue to green emission intensities changes with the excitation intensity. This is attributed to the quantum tunneling effect of carriers between the two groups of QW's and to the competition between carrier tunneling and band-to-band recombination. As for electroluminescence measurements, two distinct emissions are observed and the green emission intensity is lower than the blue emission intensity. The ratio of the two emission intensities is independent of the injected current, i.e., the color of the light does not vary with injection current.

The luminous efficacy of a broadened dichromatic white-light source is calculated assuming a line broadening ranging from $2kT$ to $10kT$, which is a typical emission linewidth in semiconductors. The calculation shows that very high values of the luminous efficiency of 219 lm/W can potentially be reached with 50% power-efficient dichromatic LED's. Such dichromatic white-light sources are suitable for many applications, in particular direct-line-of-sight applications.

ACKNOWLEDGMENTS

This work was supported in part by the NSF (Dr. U. Varshney), DARPA/ARO (Dr. J. Carrano and Dr. J. Zavada), and the ONR/University of New Mexico (Dr. Wood and Dr. Hersee).

[1] S. Nakamura and G. Fasol, The Blue Laser Diode (Springer, Berlin, 1997), pp. 216–219.
[2] R. Mueller-Mach, G. Mueller, M. Krames, and T. Trottier, IEEE J. Sel. Top. Quantum Electron. **8**, 339 (2002).
[3] P. Schlotter, R. Schmidt, and J. Schneider, Appl. Phys. A: Mater. Sci. Process. **64**, 417 (1997).
[4] X. Guo, J. W. Graff, and E. F. Schubert, Tech. Dig. Int. Electron Devices Meet. **IEDM-99**, 600 (1999).
[5] D. L. MacAdam, J. Opt. Soc. Am. **40**, 120 (1950).
[6] H. F. Ivey, J. Opt. Soc. Am. **53**, 1185 (1963).
[7] G. Wyszecki and W. S. Stiles, *Color Science: Concepts and Methods, Quantitative Data and Formulae* (Wiley, New York, 1982).
[8] W. A. Thornton, J. Opt. Soc. Am. **61**, 1155 (1971).
[9] P. Lefebvre, J. Allègre, B. Gil, A. Kavokine, H. Mathieu, W. Kim, A. Salvador, A. Botchkarev, and Hadis Morkoç, Phys. Rev. B **57**, R9447 (1998).
[10] S.-W. Feng, Y.-C. Cheng, Y.-Y. Chung, C. C. Yang, Y.-S. Lin, C. Hsu, K.-J. Ma, and J.-I. Chyi, J. Appl. Phys. **92**, 4441 (2002).
[11] J. F. Muth, J. D. Brown, M. A. L. Johnson, Z. Yu, R. M. Kolbas, J. W. Cook, Jr., and J. F. Schetzina, MRS Internet J. Nitride Semicond. Res. **4S1**, G5.2 (1999).
[12] M. Yamada, Y. Narukawa, and T. Mukai, Jpn. J. Appl. Phys., Part 2 **41**, L246 (2002).
[13] E. F. Schubert, *Light-Emitting Diodes* (Cambridge University Press, Cambridge, U.K., 2003).
[14] D. K. Schroder, IEEE Trans. Electron Devices **44**, 160 (1997).
[15] X. Guo and E. F. Schubert, J. Appl. Phys. **90**, 4191 (2001).
[16] S. Dalmasso, B. Damilano, C. Pernot, A. Dussaigne, D. Byrne, N. Grandjean, M. Leroux, and J. Massies, Phys. Status Solidi A **192**, 139 (2002).